γ-(S)-Guanidinylmethyl Modified Triplex-Forming Peptide Nucleic Acids Increase Hoogsteen-Face Affinity for a MicroRNA and Enhance Cellular Uptake

Article *in* ChemBioChem · June 2019

DOI: 10.1002/cbic.201900393

CITATIONS
5

READS
112

4 authors, including:

Ville Tähtinen
University of Turku
12 PUBLICATIONS **37** CITATIONS
SEE PROFILE

Alejandra Verhassel
University of Turku
4 PUBLICATIONS **8** CITATIONS
SEE PROFILE

Pasi Virta
University of Turku
94 PUBLICATIONS **1,040** CITATIONS
SEE PROFILE

ChemPubSoc Europe

DOI: 10.1002/cbic.201900393

CHEMBIOCHEM Full Papers

γ-(*S*)-Guanidinylmethyl-Modified Triplex-Forming Peptide Nucleic Acids Increase Hoogsteen-Face Affinity for a MicroRNA and Enhance Cellular Uptake

Ville Tähtinen,*[a] Alejandra Verhassel,[b] Johanna Tuomela,[b] and Pasi Virta*[a]

γ-Modified (i.e., (*S*)-aminomethyl, (*S*)-acetamidomethyl, (*R*)-4-(hydroxymethyl)triazol-1-ylmethyl, and (*S*)-guanidinylmethyl) triplex-forming peptide nucleic acids (TFPNAs) were synthesized and the effect of the backbone modifications on the binding to a miR-215 model was studied. Among the modifications, an appropriate pattern of three γ-(*S*)-guanidinylmethyl modifications increased the affinity and Hoogsteen-face selectivity for the miR-215 model without ternary $(PNA)_2$/RNA complex formation. Moreover, the γ-(*S*)-guanidinylmethyl groups were observed to facilitate internalization of the TFPNAs into living PC-3 prostate cancer cells.

Introduction

In recent years, there has been increasing interest in the molecular recognition of double-stranded RNA to control the function of noncoding RNAs.[1–4] A large number of noncoding RNAs (including many microRNAs[5]) are either completely double-stranded or contain short double-stranded regions. The recognition of such regions by triplex-forming oligonucleotides (TFOs) would allow sequence-selective targeting through Hoogsteen base pairing.[6] However, the binding affinity of TFOs for double-stranded RNA is usually modest. Compared to TFOs, triplex-forming peptide nucleic acids (TFPNAs) have been shown to have remarkably higher affinity for double-stranded RNA.[7–20] TFPNAs that contain naturally occurring nucleobases can target purine-rich RNA strands, where binding takes place through hydrogen bonding between T/U*A–U and C^+*G–C triplets.[6,21–25] The C^+*G–C triplet requires protonation at the cytosine-N^3 ($pK_a \approx 4.5$) and the binding with guanosine-containing targets is hence limited to acidic conditions. Moreover, the binding of unmodified PNAs may show modest selectivity between the single-stranded and double-helical RNA and the corresponding DNA targets. To facilitate binding at physiological conditions and to improve the selectivity for double-helical RNA, TFPNAs with artificial nucleobases have been extensively studied. For example, replacing cytosine with a more basic 2-aminopyridine ($pK_a = 6.7$), introduced by Rozners et al., facilitates binding of TFPNAs at physiological pH.[14] Within this modification, the PNA/RNA triplexes were also noted to be more stable than the corresponding PNA/DNA triplexes, and additionally facilitated cellular uptake of the PNAs has been reported.[10] The efficient recognition of pyrimidine inversions that often exist in double-helical RNA is still the major limitation of the triple-helical recognition. Promising binders, able to recognize pyrimidines from the Hoogsteen face (or the whole base pair), have also been developed.[6,13,26]

Incorporating chiral units into the backbone of PNAs may provide suitable preorganization that improves binding affinity and selectivity for RNA targets. Various studies have assessed the binding of chiral PNAs to single-stranded RNAs,[27–34] but the attempts to recognize double-helical RNA by chiral PNAs are limited to only two recent reports.[15,35] Gupta et al.[15] studied the binding of α-guanidine-modified PNAs (α-GPNAs) to double-helical RNA. The α-GPNAs had reduced affinity and sequence selectivity for RNA hairpins. The data also suggested that α-GPNA preferred a ternary 2:1 $(PNA)_2$/RNA triplex invasion complex instead of a stoichiometric PNA/RNA triplex. Recently, we studied the binding of TFPNAs to stem regions of ^{19}F-labeled RNA hairpin models that allowed detection of the binding by ^{19}F NMR spectroscopy.[35] The ^{19}F NMR spectroscopic analysis revealed detailed information on the stoichiometry and transition between alternative binding modes, that is, stoichiometric 1:1 PNA/RNA triplex and ternary 2:1 $(PNA)_2$/RNA triplex invasion complex. We introduced γ-(*R*)-hydroxymethyl modifications into TFPNAs and noticed that an appropriate pattern of γ-(*R*)-hydroxymethyl modifications reduced the extent of the ternary $(PNA)_2$/RNA invasion complex and preferred stoichiometric Hoogsteen-face binding to the miR-215 model.

The present study examines whether the γ substitutions could be used to further increase the Hoogsteen-face affinity of TFPNAs. γ-(*R*)-Azidomethyl modifications were introduced into variable positions of a TFPNA targeting the double-helical

[a] *V. Tähtinen, Prof. P. Virta*
Department of Chemistry, University of Turku
Vatselankatu 2, 20014 Turku (Finland)
E-mail: vpotah@utu.fi
pamavi@utu.fi

[b] *A. Verhassel, Dr. J. Tuomela*
FICAN West Cancer Research Laboratory
University of Turku and Turku University Hospital
Institution of Biomedicine, Medisiina D
Kiinamyllynkatu 10, 20520 Turku (Finland)

Supporting information and the ORCID identification numbers for the authors of this article can be found under https://doi.org/10.1002/cbic.201900393.

stretch of the miR-215 hairpin. The azidomethyl groups were postsynthetically converted into different γ substituents ((*S*)-aminomethyl, (*S*)-acetamidomethyl, (*R*)-4-(hydroxymethyl)triazol-1-ylmethyl, and (*S*)-guanidinylmethyl) and their effect on the binding to miR-215 was studied. Among the γ modifications incorporated, guanidinylmethyl groups would have the potential to increase the binding affinity and cellular uptake of TFPNAs, whereas the aim of the other modifications was rather to show, how the binding tolerates these structures to be applied for further synthetic design of TFPNAs. As mentioned above, guanidine modifications at the α-position have been reported to lower the affinity and sequence selectivity of TFPNAs and to prefer ternary 2:1 $(PNA)_2$/RNA triplex invasion complexes.[15] However, encouraged by our previous report,[35] we envisioned that the guanidinylmethyl modifications at the γ-position would potentially provide favorable preorganization, together with stabilizing charge interaction, without marked steric hindrance for triplex formation. The effect of the γ-(*S*)-guanidinylmethyl groups on the cellular delivery of TFPNAs was additionally studied. For this purpose, the TFPNAs were labeled with a HiLyte Fluor 488 (HF488) dye and their internalization to living PC-3 prostate cancer cells was followed by confocal microscopy.

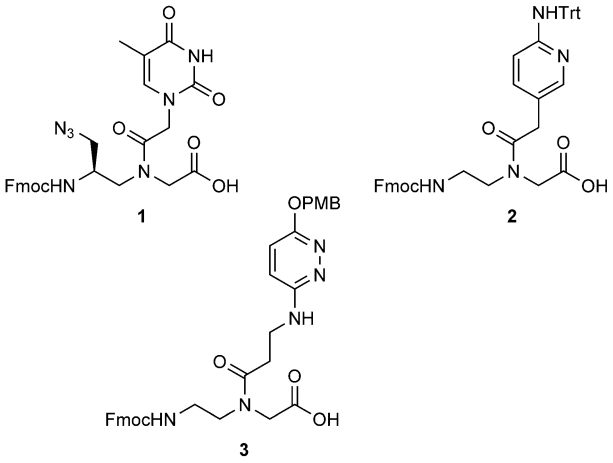

Figure 1. Modified PNA building blocks **1**–**3** used for the synthesis of TFPNAs. Trt = trityl, PMB = *p*-methoxybenzyl, Fmoc = fluorenylmethyloxycarbonyl. Compound **2** was synthesized as previously described.[14,35]

Results and Discussion

Synthesis of the PNA monomers 1–3

The modified PNA monomers **1**–**3** used for the synthesis of TFPNAs are shown in Figure 1 (see also **PNA1**–**PNA9**, Figure 2). For the incorporation of γ modifications into TFPNAs, the γ-(*R*)-azidomethyl-modified precursor **1** was synthesized and its applicability for the automated PNA assembly was demonstrated. The synthesis and applicability of the Trt-protected 2-aminopyridine monomer **2** has been described in our previous report.[35] The 3-oxo-2,3-dihydropyridazide monomer **3**, used for the recognition of UA inversion,[13,36] was protected by the *p*-methoxybenzyl (PMB) group. PMB increased the solubility of **3** in *N*-methyl-2-pyrrolidone (NMP), being beneficial for the automated PNA assembly. The syntheses of **1** and **3** are described in Scheme 1. Compound **1** was synthesized from the Weinreb amide **4**.[37] Reduction with $LiAlH_4$ gave aldehyde **5**, which was introduced to reductive amination with allyl glycinate (**6**) to yield compound **7**. The optical purity of **7** was confirmed by chiral HPLC analysis (Figure S4 in the Supporting Information). Thereafter, thymine-1-yl acetic acid was coupled to **7** by using BOP as coupling reagent, and finally Pd^0-catalyzed allyl removal gave monomer **1** (9% overall yield from **4**, four steps). For the synthesis of monomer **3**, compound **9** was converted into compound **10** by a nucleophilic aromatic substitu-

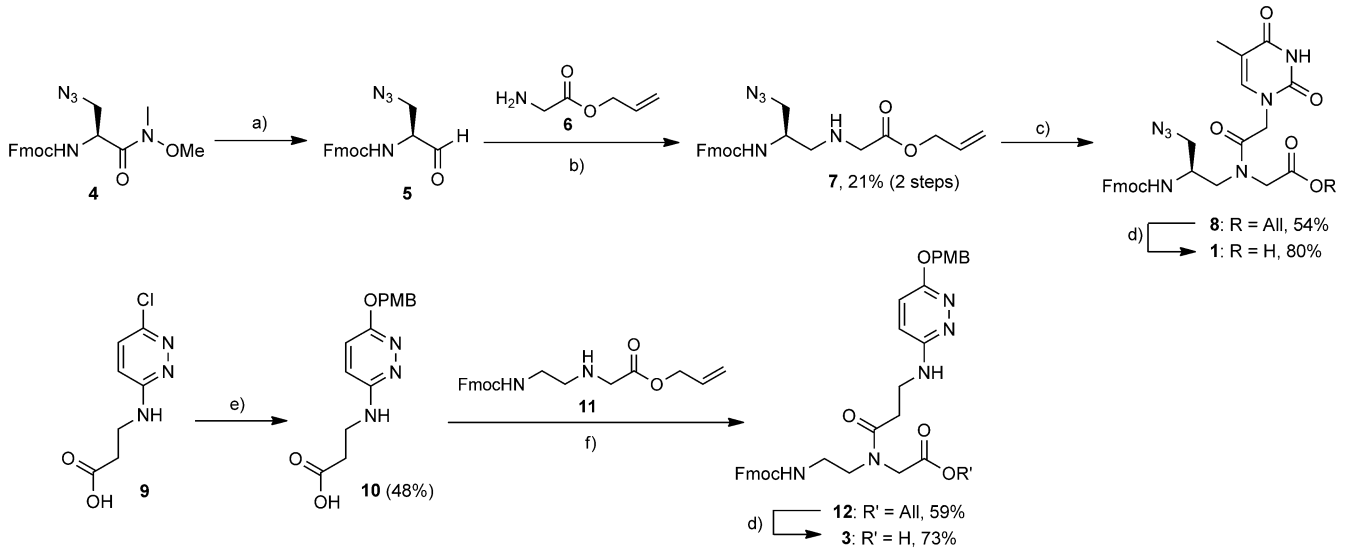

Scheme 1. a) $LiAlH_4$, THF, 30 min at RT; b) $NaBH_3CN$, AcOH/MeOH (1:99, *v*/*v*), 3 h at RT; c) thymine-1-yl acetic acid, (benzotriazol-1-yloxy)tris(dimethylamino)-phosphonium hexafluorophosphate (BOP), *N*,*N*-diisopropylethylamine (DIPEA), DMF, two days at RT; d) $[Pd(PPh_3)_4]$, phenylsilane, THF, 2–3 H; RT; e) NaH, *p*-methoxybenzyl alcohol, 1 h at 160 °C; f) BOP, DIPEA, DMF, overnight at RT.

tion with *p*-methoxybenzyl alcoxide. Compound **10** was then coupled to **11**[38] by using BOP as coupling reagent, and Pd^0-catalyzed allyl removal gave monomer **3** in 20% overall yield (from **9**, three steps). All the monomers **1**–**3** were readily soluble in NMP to provide 0.25 mol L^{-1} solutions needed for the automated PNA synthesis.

Synthesis of TFPNAs and oligonucleotides

PNA1–**PNA9** (Figure 2) were synthesized on 10 μmol scale on a Chem Matrix resin by using an automated peptide synthesizer. The PNA monomers **1**–**3**, Fmoc-PNA-T-OH, and the amino acid building blocks (Lys and Arg) were used for the assembly following a Fmoc/*t*Bu peptide synthesis cycle. Benzotriazol-1-yl-oxytripyrrolidinophosphonium hexafluorophosphate (PyBOP) was used as coupling reagent. **PNA1** was previously described by Rozners et al.[14] For the synthesis of the γ-substituted **PNA2**–**PNA8**, γ-(*R*)-azidomethyl-modified PNAs were first assembled (**SP-PNAs A**, SP = solid phase, Scheme 2). The azido groups were then converted into different modifications on the solid phase (**SP-PNAs B** and **C**): Click reaction with propargyl alcohol (TBTA, $CuSO_4$, sodium ascorbate, H_2O, DMF, overnight at RT), followed by the cleavage, afforded **PNA5**. Reduction under Staudinger conditions by using Me_3P (H_2O/dioxane (1:4, *v*/*v*), 2 h at RT), followed by the cleavage, gave **PNA3**. Acetylation (acetic anhydride, 2,6-lutidine, *N*-methylimidazole, THF, 10 min at RT), followed by the cleavage, gave **PNA4**. For the synthesis of the guanidinylmethyl-modified **PNA6**–**PNA8**, the aminomethyl groups of **SP-PNAs B** were treated with 1,3-di-Boc-2-(trifluoromethylsulfonyl)-guanidine (triethylamine, THF, RT, overnight) by following a previously described on-support guanidinylation procedure.[39] It may also be mentioned that γ-arginine-modified PNA building blocks have recently been reported and incorporated into PNAs.[40,41] For the synthesis of the HF488-labeled PNAs (**HF488-PNA6**–**HF488-PNA9**), two 2-(2-aminoethoxy)ethoxy acetic acid (AEEA) spacers were first attached to the amino terminus of **SP-PNAs C** and the HF488 label was then manually coupled following a previously described procedure.[42] The solid-supported PNAs (**SP-PNAs A–D**) were released with a mixture of anisole and trifluoroacetic acid, precipitated in Et_2O and purified by reverse-phase (RP) HPLC. The authenticity of the products was verified by MS (ESI-TOF, see Figures S25–S37 and Tables S1 and S2).

The oligonucleotides were synthesized on 1.0 μmol scale by using an automatic DNA/RNA synthesizer. The ^{19}F-labeled miR-215 model (**ORN3**, Figure 5) was synthesized by using a 2′-*O*-[(4-CF_3-triazol-1-yl)methyl]uridine-derived phosphoramidite building block as previously described by our group.[43]

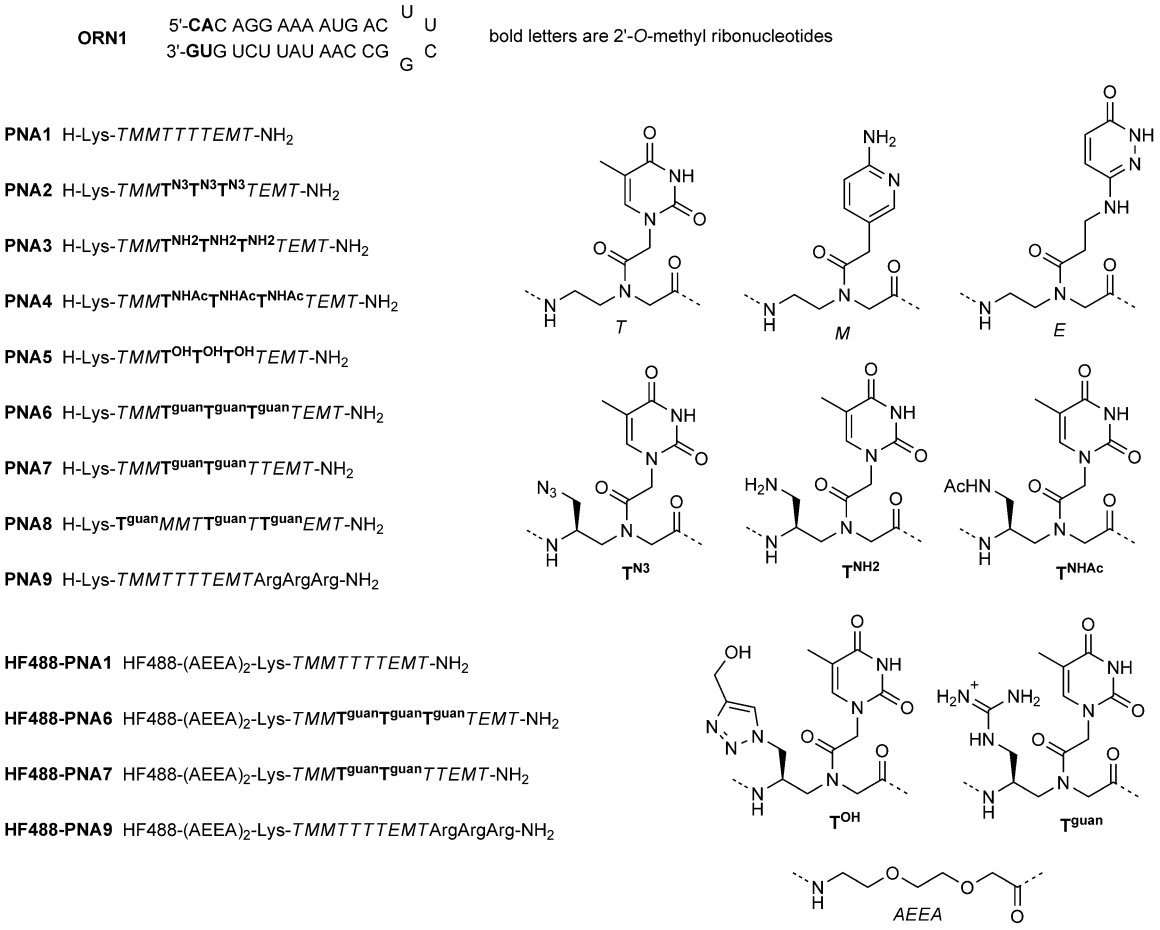

Figure 2. Structures of the miR-215 model **ORN1** and the TFPNAs studied herein.

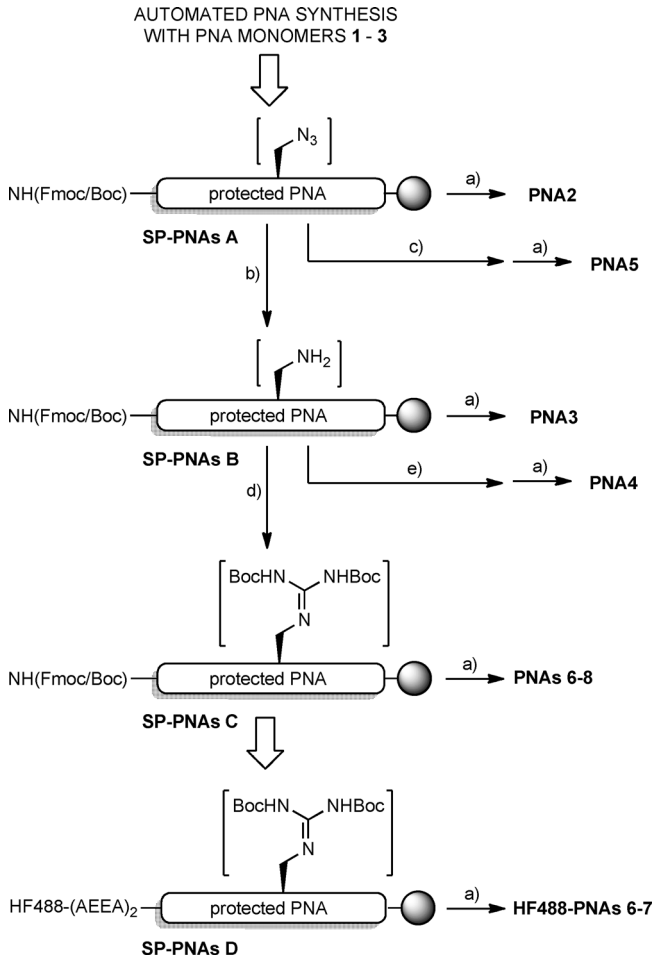

Scheme 2. Synthesis of **PNA2**–**PNA8** and **HF488-PNA6**–**PNA7**. a) Anisole/trifluoroacetic acid (TFA; 1:10, *v/v*), 2 H; RT; b) Me_3P, H_2O/dioxane (1:4, *v/v*), 2 h at RT; c) propargyl alcohol, tris((1-benzyl-4-triazolyl)methyl)amine (TBTA), $CuSO_4$, sodium ascorbate, H_2O, DMF, overnight, RT; d) 1,3-di-Boc-2-(trifluoromethylsulfonyl)-guanidine (Boc = butyloxycarbonyl), triethylamine, THF; e) acetic anhydride, 2,6-lutidine, *N*-methylimidazole, THF, 10 min at RT.

Table 1. UV thermal melting temperatures [°C] of the miR-215 model **ORN1** in the presence of 0 (T_m1 value) or 1.0 equiv (T_m2 values) of TFPNAs.

	T_m1	T_m2[a]
ORN1 alone	54.4 ± 0.6	
ORN1 + **PNA1**		60.9 ± 0.3[a]
ORN1 + **PNA2**		55.7 ± 0.6 (−5.2)[a]
ORN1 + **PNA3**		58.3 ± 1.1 (−2.6)[a]
ORN1 + **PNA4**		56.8 ± 0.4 (−4.1)[a]
ORN1 + **PNA5**		57.2 ± 0.4 (−3.7)[a]
ORN1 + **PNA6**		63.7 ± 0.6 (+2.8)[a]
ORN1 + **PNA7**		62.9 ± 0.3 (+2.0)[a]
ORN1 + **PNA8**		63.3 ± 0.7 (+2.4)[a]
ORN1 + **PNA9**		66.5 ± 0.4 (+5.4)[a]

Conditions: 2.0 μmol L^{-1} **ORN1** + 0 (T_m1 values) or 1.0 (T_m2 values) equiv PNA, 10 mmol L^{-1} sodium cacodylate (pH 7.0), 0.1 mol L^{-1} NaCl in H_2O. [a] ΔT_m values given in parentheses are those compared with the T_m values of **ORN1** + **PNA1**.

UV spectroscopic analysis of PNA/miR-215 triplexes

The influence of different γ substitutions on the thermal stability of the PNA/miR-215 triplex was first evaluated by UV thermal melting profile analysis. It may worth of noting that UV melting experiments alone cannot be used for the evaluation of the triplex stability because of the overlapping absorbances of the hairpin (**ORN1**) alone, the desired triple helix (**C**) and the ternary complex (**D**) (see scheme in Figure 5).[35] UV experiments were hence used for the qualitative selection of the PNAs for further analysis. The experiments were performed by using 2.0 μmol L^{-1} solutions of **ORN1** in the presence of 0 or one equivalent of the PNAs in a mixture of 10 mmol L^{-1} sodium cacodylate (pH 7.0) and 0.1 mol L^{-1} NaCl in H_2O. The thermal melting temperatures are listed in Table 1. The melting temperatures for **ORN1** alone and **ORN1** + **PNA1** were determined in our previous report.[35] As shown in Table 1, **PNA2**–**PNA5** with three consecutive γ-(*R*)-azidomethyl, γ-(*S*)-aminomethyl, γ-(*S*)-acetamidomethyl, γ-(*R*)-4-(hydroxymethyl)triazol-1-ylmethyl, or γ-(*S*)-guanidinylmethyl modifications showed 2.6–5.2 °C lower T_m values compared to **PNA1**. In our previous report, a similar pattern of γ-(*R*)-hydroxymethyl modifications also decreased the overall UV-based T_m value, but the triplex specificity to the miR-215 model was increased. Despite the decreased T_m values, the binding still tolerated rather well with these backbone modifications, which indicates that the γ site may be used for the further conjugation of TFPNAs (by using, e.g., click reactions or simple amide couplings). In contrast to **PNA2**–**PNA5**, the γ-(*S*)-guanidinylmethyl-modified **PNA6** showed a 2.8 °C higher T_m value. Because of this slightly stabilizing effect, we selected the γ-(*S*)-guanidinylmethyl modification for more detailed analysis (see the ^{19}F NMR experiments below). Binding of **PNA7** and **PNA8** was then examined. **PNA7** contains two consecutive γ-(*S*)-guanidinylmethyl units and **PNA8** contains three γ-(*S*)-guanidomethyl units separated by one to three PNA building blocks. According to UV spectroscopy, **PNA7** and **PNA8** have increased T_m values by 2.0 and 2.4 °C, respectively, compared to **PNA1**. For comparison to γ-(*S*)-guanidomethyl units, we also wanted to study how simple arginine overhang affects the binding affinity of the TFPNA. Accordingly, the binding of **PNA9** with three arginine units at the carboxyl terminus was studied. According to UV spectroscopy, **PNA9** has the highest T_m value (66.5 °C). The UV melting profiles of **ORN1** with one equivalent of **PNA1** and **PNA6**–**PNA9** are shown in Figure 3.

To study the selectivity of the γ-(*S*)-guanidomethyl- and arginine modified TFPNAs for double-helical RNA, we also examined the binding of **PNA1** and **PNA6**–**PNA9** to a miR-215 DNA derivative (**ODN1**, Figure 4), single-stranded RNA (**ORN2**), and single-stranded DNA (**ODN2**). **ORN2** and **ODN2** are, at least in theory, capable of forming a duplex with the PNAs through A–T and G–M base pairs. M-modified PNAs have previously been shown to have high selectivity for double-stranded RNA over DNA.[14] For the miR-215 DNA derivative **ODN1**, the observed UV thermal melting temperatures with all TFPNAs were approximately 20 °C lower compared to the corresponding PNA/miR-215 triplexes (Table S3). The melting temperatures for the **ORN2**/**PNA** duplexes were approximately 30 °C lower com-

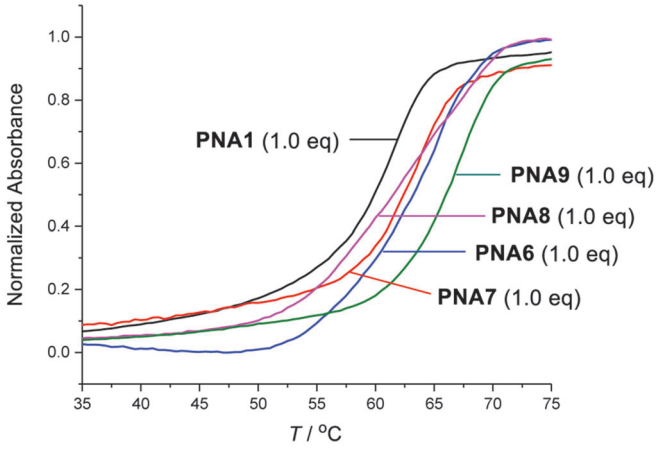

Figure 3. Normalized UV melting profiles of **PNA6**–**PNA9**/miR-215 triplexes. Conditions: 2.0 μmol L^{-1} **ORN1** + 1.0 equiv **PNA1**, **PNA6**, **PNA7**, **PNA8**, or **PNA**, 10 mmol L^{-1} sodium cacodylate (pH 7.0), 0.1 mol L^{-1} NaCl in H_2O.

5'-CAC AGG AAA ATG AC T T
3'-GTG TCT TAT AAC CG G C

ODN1

5'-AGU AAA AGG A-3'

ORN2

5'-AGT AAA AGG A-3'

ODN2

Figure 4. Structures of the miR-215 DNA derivative (**ODN1**), single-stranded RNA (**ORN2**), and single-stranded DNA (**ODN2**).

pared to the PNA/miR-215 triplexes (Table S4) and the thermal stabilities of the **ODN2**/**PNA** duplexes were even lower (data not shown here). The γ-(*S*)-guanidomethyl and arginine modifications increased the stabilities of all the complexes, as may be expected due to their positive charge. However, the affinity of the TFPNAs for **ODN1**, **ODN2**, and **ORN2** remained remarkably weak compared to miR-215. In conclusion, the γ-(*S*)-guanidomethyl-modified TFPNAs maintained the selectivity for double-stranded RNA.

^{19}F NMR spectroscopic analysis of PNA/miR-215 triplexes

To examine the binding of the γ-(*S*)-guanidinylmethyl-modified **PNA6**–**PNA9** to miR-215 in more detail, we utilized ^{19}F NMR spectroscopy. In our previous report,[35] we analyzed the binding of **PNA1** (Figure 2) to the miR-215 model **ORN3** labeled with a 2′-*O*-[(4-CF_3-triazol-1-yl)methyl]uridine sensor[43,44] (Figure 5). Our ^{19}F NMR spectroscopic analysis revealed detailed information on the stoichiometry and transition between alternative binding modes, that is, stoichiometric 1:1 PNA/RNA triplex (**C**, Figure 5) and ternary 2:1 $(PNA)_2$/RNA triplex invasion complex (**D**, Figure 5). For comparison, the previously reported ^{19}F NMR spectra of **ORN3** in the presence of 0–2.0 equivalents of **PNA1** at 40 °C are shown in Figure 5 A. The ^{19}F NMR spectra of **ORN1** in the presence of one equivalent of **PNA1** at temperatures 40–70 °C are shown in Figure 6 A, and the corresponding relative peak areas of the ^{19}F resonance signals as a function of temperature in Figure 6 B. Based on these relative peak areas, thermal denaturation profiles and distinct melting temperatures could be determined for both complexes: **C**: T_m2 = (58.9 ± 0.7) °C and **D**: T_m3 = (69.9 ± 0.2) °C. In the present study,

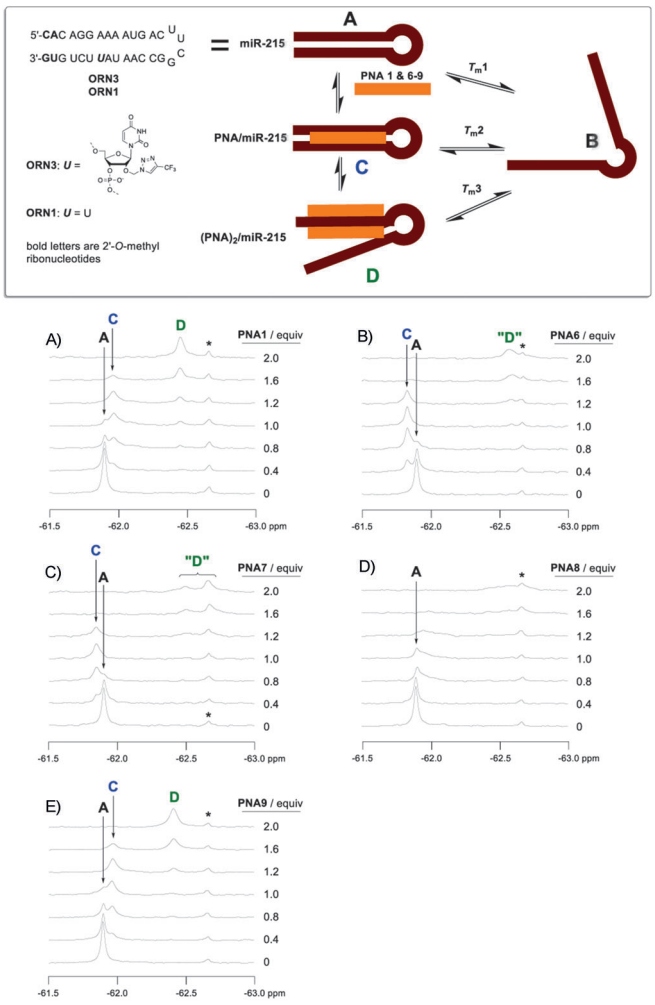

Figure 5. Titration of the miR-215 model **ORN3** with **PNA1** and **PNA6**–**PNA9** followed by ^{19}F NMR spectroscopy. Conditions: 50 μmol L^{-1} **ORN3** + PNA (0–2.0 equivalents), 10 mmol L^{-1} sodium cacodylate (pH 7.0), 0.1 mol L^{-1} NaCl in D_2O/H_2O (1:9, *v/v*). Notes: A–E) δ(**A**) = −61.90 ppm, * = single-stranded trace, δ = −62.67 ppm; A) δ(**C**) = −61.97, δ(**D**) = −62.56 ppm; B) δ(**C**) = −61.83, δ(**D**) = −62.58 ppm; C) δ(**C**) = −61.85, δ(**D**) = −62.34 to −62.82 ppm; E) δ(**C**) = −61.97, δ(**D**) = −62.41 ppm. A) Reprinted and modified with permission from reference [35].

we wanted to examine how the γ-(*S*)-guanidinylmethyl modifications affect the binding stoichiometry of the TFPNAs and the thermal stabilities of complexes **C** and **D**.

First, the binding of **PNA6**, containing three consequent γ-(*S*)-guanidinylmethyl modifications, was monitored. The ^{19}F NMR spectra of **ORN3** in the presence of 0–2.0 equivalents of **PNA6** at 40 °C are shown in Figure 5 B. **ORN3** alone gave a signal at δ = −61.90 ppm (**A**). Titration of **ORN3** with **PNA6** resulted in a new signal at −61.83 ppm, indicating the formation of the **PNA6**/**ORN3** triplex **C**. When more than one equivalent of **PNA6** was added, this signal was replaced by a broad signal at δ = −62.58 ppm. This signal may be attributed to the unspecific formation of the ternary $(PNA6)_2$/**ORN3** complex (**D**). According to the relative peak areas of the ^{19}F resonance signals, complex **C** followed 1:1 stoichiometry and complex **D** 2:1 stoichiometry. Next, ^{19}F NMR spectroscopic melting profile for the

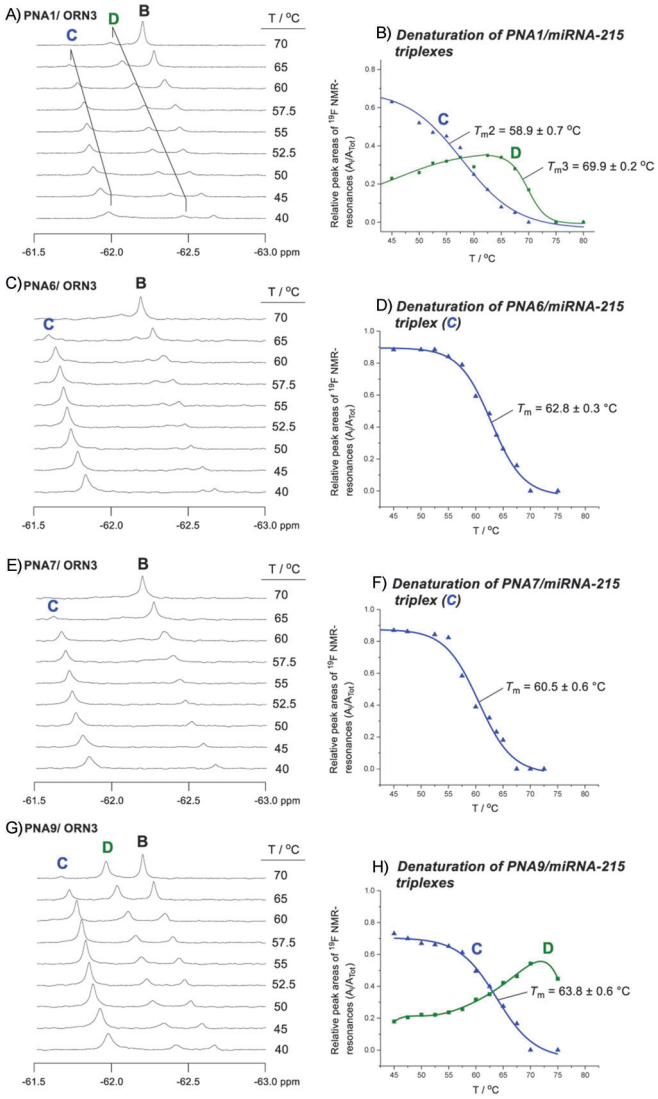

Figure 6. The thermal unwinding of PNA/miR-215 complexes monitored by ^{19}F NMR spectroscopy. Conditions: 50 μmol L^{-1} **ORN3** + **PNA1** and **PNA6**–**PNA9** (G, H: 1.25 equiv; others: 1.0 equiv), 10 mmol L^{-1} sodium cacodylate (pH 7.0), 0.1 mol L^{-1} NaCl in D_2O/H_2O (1:9, *v/v*). A,B) Reprinted and modified with permission from reference [35]; copyright: 2017, Wiley-VCH.

PNA6/**ORN3** triplex was determined. ^{19}F NMR spectra of **ORN3** in the presence of one equivalent of **PNA6** at temperatures 40–70 °C are shown in Figure 6C, and the corresponding melting profile in Figure 6D. The ^{19}F NMR spectroscopy-based melting temperature for the **PNA6**/**ORN3** triplex was (62.8 ± 0.3) °C, 3.9 °C higher compared to the original **PNA1**/**ORN3** triplex. Moreover, in contrast to **PNA1**, only trace amounts of the ternary complex **D** could be observed even at elevated temperatures.

PNA7, containing two consequent γ-(*S*)-guanidinylmethyl modifications, behaved in a similar manner (Figure 5C). As with **PNA6**, the **PNA7**/**ORN3** triplex was formed quite quantitatively up to addition of one equivalent of **PNA7** (resonance signal at $\delta = -61.85$ ppm), without the formation of the (**PNA7**)$_2$/**ORN3** complex **D**. The addition of more than one equivalent of **PNA7** gave rise to broad and undefined resonances attributed to the unspecific formation of the complex **D** (resonances between $\delta = -62.34$ and -62.82 ppm). The ^{19}F NMR spectra of **ORN3** in the presence of one equivalent of **PNA7** at temperatures 40–70 °C and the ^{19}F NMR spectroscopy-based melting profile are shown in Figure 6E and F. The ^{19}F NMR spectroscopy-based melting temperature for the **PNA7**/**ORN3** triplex was (60.5 ± 0.6) °C, 1.6 °C higher compared to the **PNA1**/**ORN3** triplex. No notable formation of the triplex invasion complex was observed even at higher temperatures.

Interestingly, titration of **ORN3** with **PNA8,** with three γ-(*S*)-guanidomethyl modifications separated by one to three PNA building blocks, resulted in a very wide dispersion of the ^{19}F resonance signals between $\delta = -61.83$ and -62.18 ppm, indicating unspecific formation of the complex **C** (Figure 5D). When more than one equivalent of **PNA8** was added, this signal pattern was replaced by broad and undefined resonances between -62.34 and $\delta = -62.63$ ppm, indicating unspecific formation of the complex **D**. Even if the formation of **C** followed approximately 1:1 stoichiometry and the formation of **D** approximately 2:1 stoichiometry, the wide dispersion of the ^{19}F resonance signals suggests unspecific and undefined binding to the **ORN3** target. Because of the wide dispersion of the signals, the melting temperatures could not be determined from NMR data.

Finally, we wanted to study how simple arginine overhang affects the binding affinity and the Hoogsteen-face selectivity of the TFPNA compared to γ-(*S*)-guanidylmethyl units. For this purpose, **PNA9** with three arginine units at the carboxyl terminus was applied. The titration of **ORN3** with **PNA9** showed very similar results compared to **PNA1** (Figure 5E). First, a signal at $\delta = -61.97$ ppm, attributed to the formation of complex **C**, was observed. The addition of more than 0.8 equivalents of **PNA9** gave rise to a signal at $\delta = -62.41$ ppm, indicating the formation of complex **D**. The ^{19}F NMR spectra of **ORN3** in the presence of one equivalent of **PNA9** at temperatures 40–70 °C are shown in Figure 6G. The corresponding relative peak areas of the ^{19}F resonance signals plotted as a function of temperature are shown in Figure 6H. The melting temperature for complex **C** was (63.8 ± 0.6) °C, 4.9 °C higher compared to the original **PNA1**/**ORN3** triplex. However, the molar fraction of the ternary triplex invasion complex **D** increased at higher temperatures and **D** became the predominant complex at $T >$ 63 °C. As a matter of fact, the arginine overhang proved to stabilize complex **D** even more than complex **C**: the melting temperature for complex **D** was (78.0 ± 0.4) °C, 7.7 °C higher compared to **PNA1** (Figure S38 and Table 2). All the ^{19}F NMR spectroscopy-based thermal melting temperatures are listed in Table 2. It may be worth mentioning that T_m3 values with two equivalents of **PNA6**–**PNA8** could not be extracted because of the broad signals of the ternary complexes.

Comparison of the results obtained by UV and ^{19}F NMR spectroscopy

The UV spectroscopic thermal melting studies showed that the γ-(*S*)-guanidomethyl-modified **PNA6**–**PNA8** and **PNA9** with an arginine overhang all stabilized the PNA/miR-215 triplex com-

Table 2. ^{19}F NMR spectroscopy-based thermal melting temperatures [°C] of the miR-215 model **ORN3** in the presence of 0 (T_m1 value), 1.0 (T_m2 values), or 2.0 equiv (T_m3 values) TFPNAs.

	T_m1	T_m2[a]	T_m3[b]
ORN3 alone	53.3 ± 0.4		
ORN3 + **PNA1**		58.9 ± 0.7[a]	70.3 ± 0.4[b]
ORN3 + **PNA6**		62.8 ± 0.3 (+3.9)[a]	n.d.
ORN3 + **PNA7**		60.5 ± 0.6 (+1.6)[a]	n.d.
ORN3 + **PNA8**		n.d.	n.d.
ORN3 + **PNA9**		63.8 ± 0.6 (+4.9)[a]	78.0 ± 0.4 (+7.7)[b]

Conditions: 50 μmol L^{-1} **ORN3** + 0 (T_m1 values), 1.0 (T_m2 values), or 2.0 equiv (T_m3 values) PNA, 10 mmol L^{-1} sodium cacodylate (pH 7.0), 0.1 mol L^{-1} NaCl in D_2O/H_2O (1:9, *v/v*). [a] ΔT_m values given in parentheses are those compared with T_m values of **ORN3** + 1.0 equiv **PNA1**. [b] ΔT_m values given in parentheses are those compared to the T_m values of **ORN3** + 2.0 equiv **PNA1**. n.d. = melting temperature could not be determined because of the wide dispersion of the ^{19}F resonance signals.

pared to **PNA1**. The increased binding affinity is likely to result from the positive charge of the γ-(*S*)-guanidinylmethyl and arginine residues at neutral pH. The largest stabilization was obtained by **PNA9**, $\Delta T_m = 5.4$ °C. However, according to the ^{19}F NMR spectroscopic studies, the molar fraction of the (**PNA1**)$_2$/miR-215 and (**PNA9**)$_2$/miR-215 complexes increased at higher temperatures (Figure 6). This fact remains hidden in the UV thermal melting profiles. Accordingly, the observed melting profiles with **PNA1** and **PNA9** are a sum of the melting profiles of both complexes **C** and **D**. Therefore, a falsely high T_m value may be expected with **PNA1** and **PNA9**. With **PNA6** and **PNA7**, on the other hand, the ^{19}F NMR spectroscopic measurements showed that practically only PNA/miR-215 triplex is formed after the addition of one equivalent of PNA even at high temperatures. Hence, it might be reasonable to confirm that the UV melting profiles with **PNA6** and **PNA7** present the denaturation of PNA/miR-215 triplex only. Interestingly, the UV thermal melting temperature with **PNA8** was very close to that with **PNA6**, although the formation of the **PNA8**/miR-215 complexes resulted in a wide dispersion of ^{19}F resonance signals. The ^{19}F NMR spectroscopic results suggest that even if the T_m determined by UV spectroscopy was relatively high, the formation of the **PNA8**/miR-215 triplex was unspecific and undefined compared to other PNAs.

The increased Hoogsteen-face selectivity of **PNA6** and **PNA7** versus **PNA1** and **PNA9** is likely to originate from the γ-chiral backbone modification that provides favorable preorganization for right-handed helical conformation.[28,32,45] The increased affinity of **PNA9**, with similar preference to triplex (**C**) and ternary complex (**D**) formation compared to electrostatic interactions only. However, the reason for the obscure binding of **PNA8** remained unclear. These hardly predictable binding behaviors suggest that fine-tuning of the PNA backbone should be case-specifically designed to gain the best binders for double-helical RNA targets. A slightly increased affinity of electrostatic origin tends to dilute in increased ionic strength.[46] Therefore, it may be underlined that not the observed affinity alone, but this together with the Hoogsteen-face selectivity (obtained, e.g., by **PNA6** and **PNA7**), is important to avoid plausible off-target effects related to TFPNAs.

As in our previous report, the thermal melting studies of PNA/miR-215 complexes were also performed by using CD spectroscopy, but no convincing discrimination between different binding modes, due to severe overlapping of the profiles, could be gained.[35] The melting temperatures extracted from UV and CD spectroscopy were nearly the same.

Cellular uptake studies

To investigate the effect of the γ-(*S*)-guanidylmethyl modifications on the cellular uptake of PNAs, **PNA1**, **PNA6**, **PNA7**, and **PNA9** were selected and labeled at the amino terminus with HiLyte Fluor 488 (HF488) dye following a previously described protocol (**HF488-PNAs**, Figure 2).[42] **PNA8** was not selected for the cellular uptake studies, because the ^{19}F NMR analysis suggested unspecific binding to the miR target compared to **PNA6** and **PNA7**. Several previous reports have demonstrated that guanidinium-based side chains improve the cellular delivery of PNAs.[29,30,33,34] The cellular internalization of the PNAs to living PC-3 prostate cancer cells was followed by confocal microscopy. The cells were incubated with 5 μmol L^{-1} concentration of the HF488-labeled PNAs in Opti-MEM (without serum) in the absence of transfection agents for 36–48 h at 37 °C, 5% CO_2. After incubation, the cells were washed with Opti-MEM and incubated with Hoechst 33342 to distinguish nuclei.

At 5 μmol L^{-1} concentration, **PNA6**, **PNA7**, and **PNA9** were able to penetrate through cell membrane, which was detected as positive fluorescent signal in cytoplasm (Figure 7). The fluorescent intensity increased in the order **PNA7** < **PNA6** < **PNA9.** **PNA1**, on the other hand, showed no signal at 5 μmol L^{-1} concentration. The cellular uptake of **PNA1** could be detected after increasing the concentration to 10 μmol L^{-1} (data not shown). Hnedzko et al. previously demonstrated that the M nucleobase modification and arginine conjugates both improve the cellular uptake of PNAs.[10] Our data shows that the γ-(*S*)-guanidylmethyl modifications enhance the cellular delivery of PNAs, albeit the enhancement was lower compared to arginine conjugates (see **PNA6** with three γ-(*S*)-guanidylmethyl groups vs. **PNA9** with three arginine conjugates). The γ-(*S*)-guanidylmethyl modification and arginine both bear a guanidine head group that has been demonstrated to be the critical component for the more efficient cellular uptake of arginine oligomers compared to other polycationic oligomers.[47]

Conclusion

γ-Modified (i.e., (*S*)-aminomethyl, (*S*)-acetamidomethyl, (*R*)-4-(hydroxymethyl)triazol-1-ylmethyl, and (*S*)-guanidinylmethyl) TFPNAs were synthesized and the effect of the backbone modifications on the binding to a miR-215 model was studied. Among the modifications, an appropriate pattern of γ-(*S*)-guanidylmethyl groups increased the binding affinity and Hoogsteen-face selectivity to the miR-215 model. The thermal stability of the PNA/miR-215 triplex could be enhanced by inserting two and three consecutive γ-(*S*)-guanidylmethyl units in the

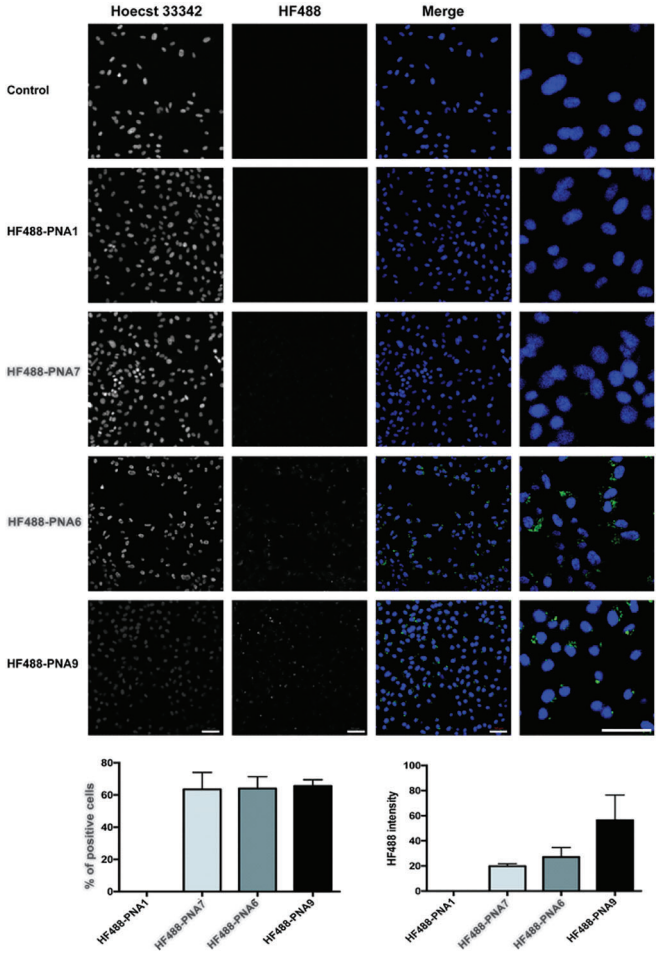

Figure 7. PNA uptake by PC-3 cells. Cells were incubated with 5 μM PNAs in Opti-MEM for 36–48 h at 37 °C. Cells were washed after incubation, stained with Hoechst 33342 and detected by confocal microscope; scale bar: 50 μm.

middle of the TFPNA (**PNA7** and **PNA6**). This stabilization was observed with both UV and ^{19}F NMR spectroscopy. Moreover, ^{19}F NMR spectroscopic analysis revealed that **PNA6** and **PNA7** favored the formation of the 1:1 PNA/miR-215 triplex over the $(PNA)_2$/miR-215 ternary complex. This information remains hidden in the UV melting profiles. Interestingly, the positioning of the γ-(*S*)-guanidylmethyl units proved important for the miR-215 recognition: when three γ-(*S*)-guanidylmethyl groups were positioned further from each other (**PNA8**), undefined and unspecific triplex formation was observed. To examine the effect of a simple arginine overhang on the miR-215 recognition, **PNA9** with three arginine units at the carboxyl terminus was additionally studied. **PNA9** showed an increased thermal stability on both PNA/miR-215 triplex and $(PNA)_2$/miR-215 ternary complex, but the arginine units had no effect on the Hoogsteen-face selectivity. In conclusion, the best combination of binding affinity and Hoogsteen-face selectivity was provided by **PNA6** with three consecutive γ-(*S*)-guanidinylmethyl modifications. These results suggest that fine-tuning of the TFPNA backbone may play a marked role in the optimal recognition of double-helical RNAs. Furthermore, the γ-(*S*)-guanidinylmethyl modifications enhanced the delivery of PNAs to living PC-3 prostate cancer cells.

Experimental Section

General: DMF and THF were dried over 4 Å molecular sieves. The NMR spectra were recorded by using a 500 MHz NMR spectrometer. The chemical shifts in the ^{1}H and ^{13}C NMR spectra are given in ppm relative to the residual signal of the deuterated solvents $CDCl_3$ and $[D_6]$DMSO. ^{19}F NMR shifts are referenced to external CCl_3F. The mass spectra were recorded in ESI mode. Oligonucleotides and PNAs were purified by RP HPLC, detection at $\lambda = 260$ nm. Oligonucleotides were purified by using a semipreparative column (C_{18}, 250 mm × 10 mm, 5 μm) with a gradient elution of 0–45% acetonitrile in 0.1 mol L^{-1} triethylammonium acetate over 25 min, flow rate of 3.0 mL min^{-1}, and PNAs by using an analytical column (C-18, 250 mm × 4.6 mm, 5 μm) with a gradient elution of 0–60% acetonitrile (0.1% trifluoroacetic acid) over 25 min, flow rate 1.0 mL min^{-1}. ***CAUTION!*** $LiAlH_4$ and triethylamine trihydrofluoride are hazardous reagents and should be handled with appropriate care.

Compound 7: Compound **4**[37] (0.71 g, 1.8 mmol) was dissolved in dry THF (12 mL) and $LiAlH_4$ (0.89 mL, 2.0 mol L^{-1}/THF, 1.8 mmol) was added dropwise at 0 °C. After being stirred for 30 min at 0 °C, the reaction was quenched by addition of 1 M $KHSO_4$. THF was evaporated under reduced pressure and the aqueous layer was extracted three times with ethyl acetate. The combined organic layer was washed with brine, dried over Na_2SO_4, filtered, and evaporated to dryness. The resulting compound **5** was used for the next step without further purification. Freshly prepared **5** and **6** (as a *p*-toluenesulfonate salt; 1.1 g, 3.8 mmol) were dissolved in a 1% solution of acetic acid in methanol. $NaBH_3CN$ (0.23 g, 3.7 mmol) was added at 0 °C and the solution was stirred at room temperature for 3 h and evaporated to dryness. The residue was dissolved in ethyl acetate and washed with a saturated aqueous solution of $NaHSO_4$ and brine. The organic layer was dried over Na_2SO_4, filtered, and evaporated to dryness. The residue was purified by column chromatography on silica gel (gradient elution from 50% hexane in EtOAc to EtOAc) to yield **7** as slightly yellowish oil (0.17 g, 21%). The stereochemical purity of **7** was confirmed by chiral HPLC analysis (Figure S4). ^{1}H NMR (500 MHz, $CDCl_3$): $\delta = 7.76$ (d, 2H; $J = 7.6$ Hz), 7.61–7.57 (m, 2H), 7.39 (t, 2H; $J = 7.4$ Hz), 7.33–7.29 (m, 2H), 5.96–5.87 (m, 1H), 5.47–5.42 (br, 1H), 5.35–5.30 (m, 1H), 5.27–5.24 (m, 1H), 4.63 (d, 2H; $J = 5.8$ Hz), 4.50–4.34 (m, 2H), 4.22 (t, 1H; $J = 6.8$ Hz), 3.81 (br, 1H), 3.50 (br, 2H), 3.45–3.34 (m, 2H), 2.84–2.81, 2.71–2.69 ppm (2×m, 2H); ^{13}C NMR (125 MHz, $CDCl_3$): 172.1, 156.1, 143.9, 141.3, 131.8, 127.7, 127.1, 125.1, 120.0, 118.9, 66.8, 65.6, 52.5, 50.7, 50.4, 50.0 ppm, (47.30, 47.27); HRMS (ESI-TOF): *m/z* calcd for $C_{23}H_{25}N_5NaO_4^+$: 458.1799 $[M+Na]^+$; found: 458.1790.

Compound 8: Compound **7** (0.41 g, 0.94 mmol) and thymine-1-yl acetic acid (0.30 g, 1.6 mmol) were suspended in DMF (3 mL) and BOP (0.71 g, 1.6 mmol) and DIPEA (0.41 mL, 2.4 mmol) were added. The mixture was stirred at room temperature for two days and evaporated to dryness. The residue was dissolved in ethyl acetate and washed with 10% aqueous solution of KH_2PO_4. The organic layer was separated, washed with saturated aqueous solution of $NaHCO_3$, dried over Na_2SO_4, filtered, and evaporated to dryness. The residue was purified by column chromatography on silica gel (gradient elution from 20% hexane in EtOAc to EtOAc) to yield **8** as a white solid (0.31 g, 54%; in addition, 13% of the starting material was recovered). ^{1}H NMR (500 MHz, $CDCl_3$): $\delta = 9.63$–9.45 (m, 1H), 7.74 (d, 2H; $J = 7.4$ Hz), 7.57 (d, 2H; $J = 7.3$ Hz), 7.40–7.36 (m,

2H), 7.29 (t, 2H; J=6.8 Hz), 6.96–6.91 (m, 1H), 5.96–5.80 (m, 1H), 5.86–5.83, 5.63–5.58 (2×m, 1H), 5.39–5.19 (m, 2H), 4.69–4.52 (m, 3H), 4.46–4.28 (m, 3H), 4.24–4.15 (m, 2H), 4.06–3.90 (m, 1H), 3.76–3.69, 3.63–3.55 (2×m, 1H), 3.55–3.39 (m, 2H), 1.84, 1.83 ppm (2×s, 3H); ^{13}C NMR (125 MHz, $CDCl_3$): (168.84, 168.73), 164.3, 156.2, (151.46, 151.31), (143.71, 143.63), 141.3, 140.9, 131.3, 131.0, 127.8, 127.1, 125.0, 120.0, 119.8, 119.0, (111.0, 110.9), 67.1, 66.8, 66.2, 52.2, 51.3, 50.2, 49.8, 49.3, 49.0, 48.1, (47.16, 47.09), 12.2 ppm; HRMS (ESI-TOF): m/z calcd for $C_{30}H_{32}N_7O_7^+$: 602.2358 $[M+H]^+$; found: 602.2358.

Compound 1: Compound **8** (0.30 g, 0.50 mmol) was dissolved in dry THF (11 mL) and $[Pd(PPh_3)_4]$ (25 mg, 0.022 mmol) and phenylsilane (0.12 mL, 1.0 mmol) were added under nitrogen atmosphere. The mixture was stirred at room temperature for 3 h and evaporated to dryness. The residue was dissolved in ethyl acetate and washed three times with a saturated aqueous solution of $NaHSO_4$ and brine. The organic layer was dried over Na_2SO_4, filtered, and evaporated to dryness. The residue was purified by column chromatography on silica gel (gradient elution from 10 to 20% water in MeCN) to yield **3** as a white powder (0.22 g, 80%). ^{1}H NMR (500 MHz, [D$_6$]DMSO): δ=11.26 (br, 1H), 7.89 (d, 2H; J=7.6 Hz), 7.86–7.78 (m, 1H), 7.75–7.65 (m, 2H), 7.74 (t, 2H; J=7.4 Hz), 7.38–7.29 (m, 2H), 7.29–7.21 (m, 1H), 4.46 (s, 2H), 4.38–4.26 (m, 2H), 4.26–4.20 (m, 1H), 3.91–3.70 (m, 3H), 3.62–3.54 (m, 1H), 3.53–3.24 (m, 2H), 3.15–3.06 (m, 1H), 1.71 ppm (s, 3H); ^{13}C NMR (125 MHz, [D$_6$]DMSO): 170.9, 168.2, 164.4, 155.8, 151.1, 143.8, 142.2, 140.7, 127.6, 127.1, 125.3, 120.1, 108.0, 65.6, 52.8, 51.9, 50.0, 49.4, 47.9, 46.7, 11.9 ppm; HRMS (ESI-TOF): m/z calcd for $C_{27}H_{27}N_7NaO_7^+$: 584.1864 $[M+H]^+$; found: 584.1891.

Compound 10: Sodium hydride (2.0 g, 60% dispersion in mineral oil, 50 mmol) was dissolved in *p*-methoxybenzyl alcohol (15 mL) and the mixture was heated to 80 °C. To the resulting solution, *N*-(3-chloropyridazin-6-yl)-3-aminopropionic acid (**9**, 2.0 g, 9.9 mmol) was added and the mixture was stirred at 160 °C for 1 h. After cooling to room temperature, water was added to the reaction mixture and the aqueous phase was washed twice with dichloromethane. The pH of the aqueous phase was adjusted to 6.0 with 2 M aqueous HCl. The resulting precipitate was filtered, washed with water, and dried under vacuum overnight to yield **10** as a slightly tan powder (1.47 g, 48%). ^{1}H NMR (500 MHz, [D$_6$]DMSO): δ=7.39–7.36 (m, 2H), 6.94–6.91 (m, 2H), 6.89–6.88 (m, 2H), 6.59–6.51 (m, 1H), 5.24 (s, 2H), 3.75 (s, 3H), 3.50–3.46 (m, 2H), 2.54 ppm (t, 2H; J=6.8 Hz); ^{13}C NMR (125 MHz, [D$_6$]DMSO): 173.3, 159.0, 158.6, 155.9, 129.9, 129.2, 120.5, 119.3, 113.7, 67.1, 55.1, 37.2, 33.6 ppm; HRMS (ESI-TOF): m/z calcd for $C_{15}H_{18}N_3O_4^+$: 304.1292 $[M+H]^+$; found: 304.1286.

Compound 12: Compound **11**[38] (0.30 g, 0.79 mmol) and compound **10** (0.29 g, 0.95 mmol) were dissolved in DMF (3 mL), and BOP (0.42 g, 0.95 mmol) and DIPEA (0.30 mL, 1.7 mmol) were added. The mixture was stirred overnight at room temperature and evaporated to dryness. The residue was dissolved in ethyl acetate and washed with a 10% aqueous solution of KH_2PO_4. The organic layer was separated, washed with a saturated aqueous solution of $NaHCO_3$, dried over Na_2SO_4, filtered, and evaporated to dryness. The residue was purified by column chromatography on silica gel (gradient elution from 2 to 5% MeOH in CH_2Cl_2) to yield **12** as a yellowish solid (0.31 g, 59%). ^{1}H NMR (500 MHz, $CDCl_3$): δ=7.74 (d, 2H; J=7.6 Hz), 7.60–7.54 (m, 2H; J=7.6 Hz), 7.40–7.26 (m, 6H), 6.91–6.85 (m, 2H), 6.73–6.68 (m, 1H), 6.60–6.52 (m, 1H), 6.00–5.81 (m, 1H), 5.37–5.24 (m, 4H), 5.02–4.94 (m, 1H), 4,67-4.56 (m, 2H), 4.38–4.34 (m, 2H), 4.22–4.13 (m, 1H), 4.07–4.03 (m, 2H), 3.80, 3.79 (2×s, 3H), 3.78–3.73 (m, 2H), 3.56–3.51 (m, 2H), 3.38–3.33 (m, 2H), 2.79–2.72, 2.62–2.57 ppm (2×m, 2H); ^{13}C NMR (125 MHz, $CDCl_3$): (173.7, 173.1), (169.9, 169.3), (159.54, 159.51), 156.6, 155.4, (143.91, 143.84), 141.3, (131.5, 131.1), 130.0, (129.15, 129.08), 127.7, 127.1, 125.1, (120.77, 120.66), (120.25, 120.18), 120.0, 119.6, 119.0, 113.9, (68.29, 68.21), 66.9, 66.7, (66.5, 66.1), 55.3, 50.6, 49.4, 49.0, 47.8 ppm, (47.25, 47.22), (39.6, 39.3), (37.8, 37.5), (32.08, 31.99); HRMS (ESI-TOF): m/z calcd for $C_{37}H_{39}N_5NaO_7^+$: 688.2742 $[M+Na]^+$; found: 688.2732.

Compound 3: Compound **12** (0.31 g, 0.47 mmol) was dissolved in dry THF (11 mL) and $[Pd(PPh_3)_4]$ (20 mg, 0.017 mmol) and phenylsilane (0.12 mL, 0.95 mmol) were added under nitrogen. The mixture was stirred at room temperature for 2 h and evaporated to dryness. The residue was dissolved in CH_2Cl_2 and washed three times with a saturated aqueous solution of $NaHSO_4$ and brine. The organic layer was dried over Na_2SO_4, filtered, and evaporated to dryness. The residue was purified by column chromatography on silica gel (gradient elution from 10% to 13% water in MeCN) to yield **3** as a white powder (0.22 g, 73%). ^{1}H NMR (500 MHz, [D$_6$]DMSO): δ=7.90–7.85 (m, 2H), 7.68 (d, 2H; J=7.4 Hz), 7.43–7.28 (m, 6H), 6.94–6.81 (m, 4H), 6.76–6.70 (m, 1H), 5.22, 5.20 (2×s, 1H), 4.20 (s, 1H), 3.752, 3.745 (2×s, 1H), 3.72–3.69 (m, 2H), 3.55–3.44 (m, 2H), 3.20–3.12 ppm (m, 2H); ^{13}C NMR (125 MHz, [D$_6$]DMSO): 172.5, 159.4, 158.9, 156.5, 144.4, 141.1, 130.3, 129.7, 128.7, 127.7, 125.8, 121.0, 120.5, 119.5, 114.2, 67.6, 66.0, 55.6, 54.0, 47.6, 47.2, 38.8, 38.3, 32.3 ppm; HRMS (ESI-TOF): m/z calcd for $C_{34}H_{36}N_5O_7^+$: 626.2609 $[M+H]^+$; found: 626.2583.

Synthesis of PNAs: PNAs were synthesized on a 10 μmol scale on a Rink amide-derived Chem Matrix resin by using an Applied Biosystems 433A peptide synthesizer. For each coupling, amino acid (5 equiv; commercially available Fmoc-PNA-T-OH monomer, Boc-Lys(Boc)-OH, Fmoc-Lys(Boc)-OH, Fmoc-Arg(Pbf)-OH (Pbf=2,2,4,6,7-pentamethyl-2,3-dehydro-1-benzofuran-5-sulfonyl), and **1**–**3**, 0.25 mol L^{-1} of each pre-dissolved in NMP), PyBOP (5 equiv), and DIPEA (10 equiv), and a 30 min coupling time (at RT) were used. The coupling was followed by a capping step with an acetic anhydride treatment (Ac_2O, pyridine (Py), NMP, 1:25:25, *v/v/v*, 1 min at RT). Piperidine (20%) in NMP was used for the Fmoc deprotection (7 min at RT). Solid-supported PNAs were released with a mixture of anisole and TFA (1:10, *v/v*, 2 h at RT), precipitated in cold diethyl ether, dissolved in a 0.1% aqueous solution of TFA, and purified by RP HPLC. The product fractions were lyophilized to dryness to give the desired homogenized PNAs as white powders. The authenticity of the PNAs was verified by MS (ESI-TOF). Yields (1–13%) of the isolated products were determined from the UV absorbance at λ= 260 nm (Table S1).

Synthesis of γ-substituted PNA2–PNA8 and HF488-PNA6–HF488-PNA8: The γ-(*R*)-azidomethyl-modified **PNA2** was synthesized by automated PNA synthesis. For the synthesis of the γ-substituted **PNA3**–**PNA8**, the γ-(*R*)-azidomethyl groups of **PNA2** were converted into different modifications on solid phase. For the synthesis of **PNA5**, solid-supported **PNA2** was suspended in a mixture of propargyl alcohol (100 equiv), TBTA (5 equiv), $CuSO_4$ (5 equiv), sodium ascorbate (10 equiv), H_2O, and DMF. The suspension was shaken overnight at room temperature, after which the support was collected by filtration, washed with H_2O, DMF, MeCN, CH_2Cl_2, and MeOH and dried under vacuum. For the synthesis of **PNA3**, solid-supported **PNA2** was suspended in a mixture of water and dioxane (1:4, *v/v*) and a solution of 1 mol L^{-1} Me_3P in toluene (24 equiv/amino group) was added under nitrogen atmosphere. The suspension was shaken for 2 h at room temperature, after which the resin was filtered and washed with DMF and CH_2Cl_2 and dried under vacuum. For the synthesis of **PNA4**, solid-supported

PNA3 was suspended in a mixture of acetic anhydride, 2,6-lutidine, *N*-methylimidazole, and THF (5:5:8:82, *v/v/v/v*). The suspension was shaken for 10 min at room temperature, after which the resin was filtered and washed with DMF and CH_2Cl_2 and dried under vacuum. For the synthesis of the guanidine-modified **PNA6**–**PNA8**, solid-supported **PNA3** was suspended in dry THF and 1,3-di-Boc-2-(trifluoromethylsulfonyl)guanidine (10 equiv/amino group) and triethylamine (50 equiv/amino group) were added. Because the guanidinylation required highly basic conditions, the lysine at the amino terminus of the PNA was protected with Boc instead of Fmoc. The suspension was shaken overnight at room temperature. The guanidinylation step turned out to be sluggish, and the treatment had to be repeated to get all the amino groups guanidinylated. Thereafter, the resin was filtered, washed with DMF and CH_2Cl_2 and dried under vacuum. Finally, the PNAs were released from the solid support as described previously.

When synthesizing guanidine-modified **HF488-PNA6**–**HF488-PNA7**, the synthesis was continued after the guanidinylation step. Therefore, the lysine at the amino terminus of the PNA had to be protected with Fmoc instead of Boc. Consequently, less basic conditions (1 equiv triethylamine/amino group) were used and the treatment was repeated three times overnight.

Oligonucleotide synthesis: The oligonucleotides were synthesized on a 1.0 μmol scale by using an Applied Biosystems 3400 DNA/RNA synthesizer, as described previously.[43] Phosphoramidite building blocks of 2′-*O*-[(4-CF_3-triazol-1-yl)methyl]uridine,[43] together with the commercially available DNA and RNA building blocks, were used for the chain assembly. Benzylthiotetrazol as an activator and coupling times of 20 s (the commercially available DNA building blocks), 300 s (the commercially available RNA building blocks) and 600 s (for 2′-*O*-[(4-CF_3-triazol-1-yl)methyl]uridine building block) were used. ODNs were released from the support with concentrated ammonia (overnight at 55 °C) and ORNs with a mixture of concentrated ammonia and ethanol[48] (3:1, *v/v*, 3 h at 55 °C, overnight at RT). The silyl protecting groups of ORNs were removed by treatment with triethylamine trihydrofluoride.[49,50] The crude oligonucleotides were purified by RP HPLC to give homogenized oligonucleotides in yields of 8–24%. The authenticity of the oligonucleotides was verified by MS (ESI-TOF).

^{19}F NMR spectroscopic studies: The spectra were recorded at a frequency of 470.6 MHz, as previously described.[40,41] Typical parameters were as follows: ^{19}F excitation pulse 4.0 ms, acquisition time 1.17 s, prescan delay 6.0 ms, relaxation delay 0.8 s, and the typical number of scans was 2048. The parameters were optimized to gain signals with the longest relaxation rate. A macro command was used for the automatic temperature ramps by using a 20 min equilibration time for each temperature. The sample temperatures were calibrated by using known shifts of ethylene glycol at different temperatures. Detailed conditions of the samples are described in the figures and tables.

Cell culture and in vitro imaging: Human prostate cancer PC-3 cells were obtained from the American Tissue Type Culture Collection (Rockville, MD, USA) and cultured in Dulbecco's modified eagle medium (Lonza, Walkersville, MD USA) supplemented with 10% inactivated fetal bovine serum (iFBS, Gibco by Life Technologies Limited, Paisley, UK), 1% penicilin–streptomycin (Gibco), and 1% Glutamax (Gibco by Life Technologies Limited, Paisley, UK). 15×10^{-3} cells were plated on an 8-well Lab-Tek II Chambered Coverglass and incubated overnight at 37 °C. Cells were washed with serum-free Opti-MEM (Gibco by Life Technologies Limited, Paisley, UK) and incubated with 5 μmol L^{-1} of the HF488-labeled PNAs in Opti-MEM for 36–48 h. After incubation, cells were washed two times with Opti-MEM and incubated with 0.1 μg mL^{-1} Hoechst 33342 (ThermoFisher Scientific) for 10 min in dark. After incubation, cells were washed three times with Opti-MEM and 300 μL Opti-MEM was added to each well. Cells were observed by using a confocal microscope, which has a CO_2-, humidity- and temperature-controlled incubator for live cell imaging (Zeiss LSM780). 20× magnification and a $\lambda = 488$ nm laser were used. Nucleus count (Hoechst 33342 staining), HF488-fluorescent signal count, and intensity analysis were performed by using ImageJ 1.50i.[51]

Acknowledgements

Inês Carvalho Guedes (University of Turku) and Dr. Jouko Sandholm (Turku Bioscience) are warmly thanked for excellent technical assistance. Biocenter Finland is acknowledged for the imaging instrumentation. Financial support from the Academy of Finland (no: 308931) is acknowledged.

Conflict of Interest

The authors declare no conflict of interest.

Keywords: ^{19}F NMR spectroscopy · cellular uptake · RNA triple helices · peptide nucleic acids

[1] D. P. Bartel, *Cell* **2004**, *116*, 281 – 297.
[2] D. P. Bartel, *Cell* **2009**, *136*, 215 – 233.
[3] H. Ling, M. Fabbri, G. A. Calin, *Nat. Rev. Drug Discovery* **2013**, *12*, 847 – 865.
[4] P. A. Sharp, *Cell* **2009**, *136*, 577 – 580.
[5] G. A. Calin, C. D. Dumitru, M. Shimizu, R. Bichi, S. Zupo, E. Noch, H. Aldler, S. Rattan, M. Keating, K. Rai, et al., *Proc. Natl. Acad. Sci. USA* **2002**, *99*, 15524 – 15529.
[6] G. Devi, Y. Zhou, Z. Zhong, D.-F. K. Toh, G. Chen, *Wiley Interdiscip. Rev. RNA* **2015**, *6*, 111 – 128.
[7] M. Li, T. Zengeya, E. Rozners, *J. Am. Chem. Soc.* **2010**, *132*, 17052 – 17052.
[8] T. Zengeya, M. Li, E. Rozners, *Bioorg. Med. Chem. Lett.* **2011**, *21*, 2121 – 2124.
[9] T. Sato, Y. Sato, S. Nishizawa, *J. Am. Chem. Soc.* **2016**, *138*, 9397 – 9400.
[10] D. Hnedzko, D. W. McGee, Y. A. Karamitas, E. Rozners, *RNA* **2017**, *23*, 58 – 69.
[11] D.-F. K. Toh, K. M. Patil, G. Chen, *J. Vis. Exp.* **2017**, e56221.
[12] R. Y. Puah, H. Jia, M. Maraswami, D.-F. Kaixin Toh, R. Ero, L. Yang, K. M. Patil, A. A. Lerk Ong, M. S. Krishna, R. Sun, C. Tong, M. Huang, X. Chen, T. P. Loh, Y.-G. Gao, D. X. Liu, G. Chen, *Biochemistry* **2018**, *57*, 149 – 159.
[13] P. Gupta, T. Zengeya, E. Rozners, *Chem. Commun.* **2011**, *47*, 11125.
[14] T. Zengeya, P. Gupta, E. Rozners, *Angew. Chem. Int. Ed.* **2012**, *51*, 12593 – 12596; *Angew. Chem.* **2012**, *124*, 12761 – 12764.
[15] P. Gupta, O. Muse, E. Rozners, *Biochemistry* **2012**, *51*, 63 – 73.
[16] O. Muse, T. Zengeya, J. Mwaura, D. Hnedzko, D. W. McGee, C. T. Grewer, E. Rozners, *ACS Chem. Biol.* **2013**, *8*, 1683 – 1686.
[17] G. Devi, Z. Yuan, Y. Lu, Y. Zhao, G. Chen, *Nucleic Acids Res.* **2014**, *42*, 4008 – 4018.
[18] T. Endoh, D. Hnedzko, E. Rozners, N. Sugimoto, *Angew. Chem. Int. Ed.* **2016**, *55*, 899 – 903; *Angew. Chem.* **2016**, *128*, 911 – 915.
[19] S. K. Cheruiyot, E. Rozners, *ChemBioChem* **2016**, *17*, 1558 – 1562.
[20] C. Annoni, T. Endoh, D. Hnedzko, E. Rozners, N. Sugimoto, *Chem. Commun.* **2016**, *52*, 7935 – 7938.
[21] R. W. Roberts, D. M. Crothers, *Science* **1992**, *258*, 1463.
[22] H. Han, P. B. Dervan, *Proc. Natl. Acad. Sci. USA* **1993**, *90*, 3806 – 3810.
[23] E. Rozners, *J. Nucleic Acids* **2012**, *2012*, 1 – 8.

[24] Y. Zhou, E. Kierzek, Z. P. Loo, M. Antonio, Y. H. Yau, Y. W. Chuah, S. Geifman-Shochat, R. Kierzek, G. Chen, *Nucleic Acids Res.* **2013**, *41*, 6664 – 6673.
[25] D. Hnedzko, S. K. Cheruiyot, E. Rozners, *Curr. Protoc. Nucleic Acid Chem.* **2014**, 4.60.1 – 4.60.23.
[26] D. F. K. Toh, G. Devi, K. M. Patil, Q. Qu, M. Maraswami, Y. Xiao, T. P. Loh, Y. Zhao, G. Chen, *Nucleic Acids Res.* **2016**, *44*, 9071 – 9082.
[27] V. A. Kumar, K. N. Ganesh, *Acc. Chem. Res.* **2005**, *38*, 404 – 412.
[28] R. Corradini, S. Sforza, T. Tedeschi, F. Totsingan, A. Manicardi, R. Marchelli, *Curr. Top. Med. Chem.* **2011**, *11*, 1535 – 1554.
[29] A. Dragulescu-Andrasi, P. Zhou, G. He, D. H. Ly, *Chem. Commun.* **2005**, 244 – 246.
[30] A. Manicardi, E. Fabbri, T. Tedeschi, S. Sforza, N. Bianchi, E. Brognara, R. Gambari, R. Marchelli, R. Corradini, *ChemBioChem* **2012**, *13*, 1327 – 1337.
[31] S. N. Oyaghire, C. J. Cherubim, C. A. Telmer, J. A. Martinez, M. P. Bruchez, B. A. Armitage, *Biochemistry* **2016**, *55*, 1977 – 1988.
[32] T. Sugiyama, A. Kittaka, *Molecules* **2013**, *18*, 287 – 310.
[33] P. Zhou, M. Wang, L. Du, G. W. Fisher, A. Waggoner, D. H. Ly, *J. Am. Chem. Soc.* **2003**, *125*, 6878 – 6879.
[34] P. Zhou, A. Dragulescu-Andrasi, B. Bhattacharya, H. O'Keefe, P. Vatta, J. J. Hyldig-Nielsen, D. H. Ly, *Bioorg. Med. Chem. Lett.* **2006**, *16*, 4931 – 4935.
[35] V. Tähtinen, L. Granqvist, M. Murtola, R. Strömberg, P. Virta, *Chem. Eur. J.* **2017**, *23*, 7113 – 7124.
[36] A. B. Eldrup, O. Dahl, P. E. Nielsen, *J. Am. Chem. Soc.* **1997**, *119*, 11116 – 11117.
[37] G. Panda, N. V. Rao, *Synlett* **2004**, *2004*, 714 – 716.
[38] O. Seitz, O. Köhler, *Chem. Eur. J.* **2001**, *7*, 3911 – 3925.
[39] K. Feichtinger, H. L. Sings, T. J. Baker, K. Matthews, M. Goodman, *J. Org. Chem.* **1998**, *63*, 8432 – 8439.
[40] A. Manicardi, A. Calabretta, M. Bencivenni, T. Tedeschi, S. Sforza, R. Corradini, R. Marchelli, *Chirality* **2010**, *22*, E161 – E172.
[41] J. Elskens, A. Manicardi, V. Costi, A. Madder, R. Corradini, J. Elskens, A. Manicardi, V. Costi, A. Madder, R. Corradini, *Molecules* **2017**, *22*, 2010.
[42] D. Hnedzko, D. W. McGee, E. Rozners, *Bioorg. Med. Chem.* **2016**, *24*, 4199 – 4205.
[43] L. Granqvist, P. Virta, *J. Org. Chem.* **2015**, *80*, 7961 – 7970.
[44] L. Granqvist, P. Virta, *Chem. Eur. J.* **2016**, *22*, 15360 – 15372.
[45] A. Dragulescu-Andrasi, S. Rapireddy, B. M. Frezza, C. Gayathri, R. R. Gil, D. H. Ly, *J. Am. Chem. Soc.* **2006**, *128*, 10258 – 10267.
[46] J. Spitzer, B. Poolman, *Microbiol. Mol. Biol. Rev.* **2009**, *73*, 371 – 388.
[47] D. J. Mitchell, L. Steinman, D. T. Kim, C. G. Fathman, J. B. Rothbard, *J. Pept. Res.* **2000**, *56*, 318 – 325.
[48] J. Stawinski, R. Strömberg, M. Thelin, E. Westman, *Nucleic Acids Res.* **1988**, *16*, 9285 – 9298.
[49] R. I. Hogrefe, A. P. McCaffrey, L. U. Borozdina, E. S. McCampbell, M. M. Vaghefi, *Nucleic Acids Res.* **1993**, *21*, 4739 – 4741.
[50] E. Westmanu, R. Stromberg, *Nucleic Acids Res.* **1994**, *22*, 2430 – 2431.
[51] C. A. Schneider, W. S. Rasband, K. W. Eliceiri, *Nat. Methods* **2012**, *9*, 671 – 675.

Manuscript received: June 13, 2019
Accepted manuscript online: June 17, 2019
Version of record online: ■■ ▮▮, 0000

V. Tähtinen, A. Verhassel, J. Tuomela, P. Virta**

■■ – ■■

γ-(*S*)-Guanidinylmethyl-Modified Triplex-Forming Peptide Nucleic Acids Increase Hoogsteen-Face Affinity for a MicroRNA and Enhance Cellular Uptake

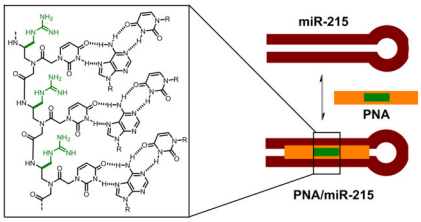

γ-(*S*)-Guanidinylmethyl-modified triplex-forming peptide nucleic acids were prepared, and the effect of the backbone modification on the binding to a micro RNA-215 model was studied. An appropriate pattern of the γ-(*S*)-guanidylmethyl groups increased the binding affinity and Hoogsteen-face selectivity. Furthermore, the γ-(*S*)-guanidinylmethyl modifications enhanced delivery of the PNAs to living PC-3 prostate cancer cells.